JOURNAL OF SOLID STATE CHEMISTRY 21, 145–154 (1977)

Structural Changes in the Solid Solution $(Ti_{1-x}V_x)_2O_3$ as x Varies from Zero to One

CATHERINE E. RICE AND WILLIAM R. ROBINSON*

Department of Chemistry, Purdue University, West Lafayette, Indiana 47907

Received October 9, 1976; in revised form January 21, 1977

The crystal structures of $(Ti_{1-x}V_x)_2O_3$, $x = 0.005$, 0.01, 0.02, 0.04, 0.07, 0.30, 0.50, 0.70, and 0.90, have been determined from X-ray diffraction data collected from single crystals. The compounds are rhombohedral, space group $R\bar{3}c$, and are isomorphous with α-alumina. The hexagonal cell dimensions range from $a = 5.1549(6)$ Å, $c = 13.627(2)$ Å, for $(Ti_{0.995}V_{0.005})_2O_3$ to $a = 4.9813(2)$ Å, $c = 13.996(1)$ Å for $(Ti_{0.10}V_{0.90})_2O_3$. The most pronounced effects of V^{3+} substitution occur in the 0 to 7 at% V range and can be described as an increase in the metal–metal distance along the c axis from 2.578(2) Å in pure Ti_2O_3 to 2.652(1) Å in $(Ti_{0.93}V_{0.07})_2O_3$ coupled with reorganization of the structure in order to maintain constant metal–oxygen distances. These structural changes have been related to both the change from semiconducting to metallic behavior and the disappearance of the 150–350°C resistivity drop which occur with increasing vanadium content in $(Ti_{1-x}V_x)_2O_3$ as x increases from 0.0 to about 0.07. They are consistent with the band theory proposed by others for this system. Indications of unusual structural behavior in the 90–100 at% V range are also noted.

Introduction

The addition of small amounts of V_2O_3 to Ti_2O_3 produces a gradual semiconductor–metal transition (*1*) much like the one observed in pure Ti_2O_3 upon heating through the 150–350°C region (*2*, *3*). Both electrical transitions are accompanied by similar distensions of the crystal lattice (*4*, *5*), and no change in space group occurs in either case. These transitions have been studied extensively by resistivity and thermoelectric measurements (*6*, *7*), specific heat measurements (*8*), Raman spectroscopy (*9*, *10*), and ultrasonic attenuation (*11*, *12*). In both cases the structural and electrical changes can be explained in terms of changes in metal–metal bond order which accompany the closing of a small gap between filled and empty d bands in the band structure of the semiconducting phase (*1*, *13*, *14*).

In addition to showing a semiconductor–metal transition, low-vanadium alloys in the $(Ti_{1-x}V_x)_2O_3$ system exhibit quite anomalous low-temperature specific heat (*15*), magnetic susceptibility (*16*, *17*), and magnetoresistance behavior (*18*). These phenomena have variously been interpreted as indicative of spin glass properties (*17*), a pseudo-one-dimensional density of states distribution (*15*), correlative effects leading to heavy polaron formation (*19*), or the existence of a narrow impurity band near the Fermi level (*20*). The role of vanadium in this system is still not well understood.

The unit cell parameters in the $(Ti_{1-x}V_x)_2O_3$ system (*5*, *21*) show drastic deviations from Vegard's Law, suggesting complexity in the intimate structural behavior. In the range 0–10% vanadium, the change in cell parameters is analogous to that observed upon heating Ti_2O_3 through its semiconductor–metal transition suggesting that the changes in $(Ti_{1-x}V_x)_2O_3$ might be analogous to those observed (*22*, *23*) in Ti_2O_3. In addition to the series of high temperature crystal structures of Ti_2O_3, the room temperature crystal structures of Ti_2O_3, $(Ti_{0.9}V_{0.1})_2O_3$, and V_2O_3

* Author to whom correspondence should be addressed.

ISSN 0022-4596

have been determined (*22–27*). However, detailed crystal structure information for intermediate concentrations has not been available. In light of the unusual structural, electrical, and magnetic behavior observed in this system, we thought it interesting to study the changes in atomic positions which occur as a function of x in $(Ti_{1-x}V_x)_2O_3$, giving special attention to the low-vanadium regime. Therefore, we have determined the crystal structures of nine such solid solutions where x varies from 0.005 to 0.90.

Experimental

Samples of $(Ti_{1-x}V_x)_2O_3$ ($x = 0.005$, 0.01, 0.02, 0.04, 0.07, and 0.10) from single-crystal boules were provided by Professor Honig of this department. The compositions of samples with $x \leqslant 0.10$ were determined by elemental analysis (*1*, *15*). The other samples were prepared by the Purdue Crystal Growth Facility by melting together the requisite amount of Ti_2O_3 and V_2O_3 in a tri-arc furnace. Past experience in this facility has shown that this technique gives Ti/V ratios within 1% of the nominal composition. Spheres with radii ranging from 0.0060 to 0.0114 cm were ground from fragments of the boules. Weissenberg photographs of representative crystals confirmed the known space group $R\bar{3}c$ (no. 167) and diffractometer measurements for all crystals were compatible with this assignment. No evidence for ordering of vanadium was found.

All crystals were mounted along nonprincipal axes to reduce the effects of multiple diffraction (*28*). Unit cell parameters and intensities were measured using an Enraf-Nonius CAD-4 diffractometer with graphite monochromated Mo$K\alpha$ radiation. Only unit cell parameters were determined for $x = 0.10$. An incident beam collimator 0.8 mm in diameter at a takeoff angle of 4.0° was used with a receiving aperture located 173 mm from the crystal. The pulse height analyzer used with the scintillation counter was set to admit approximately 95% of the diffraction intensity. Following centering of the crystal, a set of 15 reflections widely separated in reciprocal space was centered and used to determine the orientation matrix for use in intensity data collection.

Precise unit cell parameters were determined by centering the $K\alpha_1$ ($\lambda = 0.70926$ Å) peak for 50 to 60 reflections, $80° < 2\theta < 100°$, at both positive and negative 2θ and taking the average as the diffraction angle. Hexagonal cell parameters and ESDs (Table I) were calculated by least-squares refinement of the observed 2θ values using the program LCR-2 (*29*). Unit cell determinations were repeated with different crystals for several samples. In the worst case, the cell dimensions were reproducible within 8 ESDs (4 ESDs from the mean) based on the least-squares fit to the experimental data. Although the cell parameters might be susceptible to the effects of possible systematic error in the diffractometer, the differences between parameters are not.

All reflections in a hemisphere of reciprocal space with $6° < 2\theta < 66°$ were collected for all samples. The θ–2θ scanning technique with a variable scanning speed was used with a 2θ range of $1.0 + 0.2 \tan \theta$ degrees centered about the average peak position. The aperture was set at $3.0 + 2.11 \tan\theta$ mm wide by 6 mm high. Each reflection was first scanned at a rate of 20.1° min^{-1} to determine its approximate intensity. Reflections were then scanned twice at a slower rate necessary to accumulate the minimum net count of 1000 counts above background. If the results of the two slow scans were statistically different, they were repeated until agreement was reached. The maximum rate for this slower scan was 20.1° min^{-1}. Those reflections which were too weak to give the desired net count were scanned twice at 1.3° min^{-1}. The intensities of 85% of the reflections were well above the minimum count required, although the counting rates were such that no coincidence corrections were necessary. Background counts were made for $\frac{1}{4}$ of the scan time at each end of both scans. Several standard reflections were monitored every 2 hr and did not show significant intensity changes during the course of the data collection period.

Integrated intensities, I, were obtained using the expression $I = C - 2B$, where C is the sum of the counts collected during the

TABLE I

CRYSTALLOGRAPHIC DATA FOR $(Ti_{1-x}V_x)_2O_3$ WITH STANDARD DEVIATIONS IN PARENTHESES

Parameter	$x=0$[a]	0.005	0.01	0.02	0.04	0.07	0.10	0.30	0.50	0.70	0.90	1.00[b]
a_{hex} (Å)	5.1580(4)	5.1549(6)	5.1493(4)	5.1417(2)	5.1255(6)	5.1090(2)	5.1025(1)	5.0539(3)	5.0174(1)	4.9968(1)	4.9813(2)	4.9492(2)
c_{hex} (Å)	13.611(1)	13.627(2)	13.654(2)	13.686(1)	13.734(4)	13.812(1)	13.829(1)	13.953(2)	13.993(2)	13.996(1)	13.996(1)	13.998(1)
vol (Å^3)	313.6	313.6	313.5	313.3	312.5	312.2	311.8	308.6	305.1	302.6	300.8	296.9
c/a	2.64	2.64	2.65	2.66	2.68	2.70	2.71	2.76	2.79	2.80	2.81	2.83
M z	0.34485(5)	0.34484(5)	0.34503(5)	0.34519(4)	0.34563(3)	0.34602(4)	0.34614(3)[c]	0.34668(3)	0.34675(4)	0.34682(4)	0.34691(4)	0.34634(4)
β_{11}[d]	65(6)	32(4)	27(4)	28(3)	32(3)	41(4)	31(4)[c]	52(3)	41(4)	57(3)	56(3)	57(6)
β_{33}[d]	5.4(6)	4.3(5)	2.5(6)	3.8(4)	5.3(4)	4.0(5)	2.3(5)[c]	3.0(4)	3.7(5)	4.5(4)	4.4(4)	1.9(7)
Ox x	0.3133(4)	0.3130(3)	0.3130(4)	0.3126(3)	0.3122(3)	0.3120(4)	0.3114(3)[c]	0.3109(3)	0.3111(4)	0.3114(4)	0.3110(4)	0.3122(5)
β_{11}[d]	76(10)	35(6)	28(7)	27(6)	38(5)	43(7)	36(7)[c]	49(6)	33(7)	50(6)	55(7)	49(10)
β_{22}[d]	87(12)	45(9)	38(10)	37(9)	41(7)	43(9)	36(9)[c]	55(8)	52(10)	58(9)	58(10)	76(14)
β_{33}[d]	6.6(12)	4.0(10)	3.5(11)	4.2(9)	5.6(6)	5.0(8)	2.8(10)[c]	4.5(7)	4.7(8)	5.4(8)	5.7(7)	5.0(10)
β_{13}[d]	1.9(13)	1.2(10)	2.2(11)	1.5(11)	2.9(9)	3.1(10)	0.6(10)[c]	2.2(10)	3.9(11)	3.8(11)	4.1(11)	4(2)
R	0.027	0.021	0.024	0.020	0.021	0.019	0.027[c]	0.027	0.022	0.018	0.017	0.039
R_{wt}	0.030	0.024	0.032	0.027	0.024	0.029	0.030[c]	0.030	0.028	0.025	0.025	0.048
n	125	126	126	126	126	125	145[c]	122	121	121	120	98
s[e]		5.3(4)	5.5(4)	4.3(3)	3.8(3)	3.7(3)		3.2(2)	3.8(3)	1.7(2)	1.8(2)	
B_M		0.28(2)	0.21(3)	0.24(2)	0.30(2)	0.32(2)		0.34(2)	0.30(2)	0.40(2)	0.39(2)	
B_{Ox}		0.30(4)	0.25(4)	0.27(3)	0.35(3)	0.35(4)		0.38(2)	0.32(3)	0.40(2)	0.43(2)	
S		1.00	1.00	1.00	1.00	1.00		1.00	1.27	1.27	0.95	

[a] Ref. (*23*).
[b] Ref. (*26*).
[c] Ref. (*25*)
[d] Times 10^4. For M, $\beta_{11}=\beta_{22}$, $\beta_{12}=\frac{1}{2}\beta_{11}$, and $\beta_{23}=\beta_{13}=0$. For Ox, $\beta_{12}=\frac{1}{2}\beta_{22}$ and $\beta_{23}=2\beta_{13}$. The form of the anisotropic temperature factor T is $T=\exp(-\sum_I\sum_J h_I h_J \beta_{IJ})$.
[e] Times 10^5.

two slower scans, and B is the sum of the background counts during these scans. A standard deviation was assigned to each measured intensity using the expression $\sigma(I) = [C + 4B]^{1/2}$. The data were corrected for Lorentz polarization effects. The crystals were measured using a microscope with a micrometer eyepiece, and a spherical absorption correction was applied (μR for the crystals ranged from 0.48 to 0.91). Averaging of equivalent reflections gave 120 to 126 symmetry-independent reflections for each crystal. Reflections with $I < \sigma$ were set equal to $\frac{1}{2}\sigma$ and included in the refinement; there were five or six reflections in this category for each data set.

Refinement with both isotropic and anisotropic temperature factors was carried out for each set of intensity data using the RFINE2 program written by Finger (*30*). The initial atomic parameters in the space group $R\bar{3}c$ were those for Ti_2O_3 (*22*). The program minimized $\sum w(F_o - F_c)^2$ using the scattering factors for Ti^{3+}, V^{3+}, and O° (*31*) corrected for real and imaginary anomalous dispersion (*32*), weights based on average standard deviations ($w = 1/\sigma^2(F) = 4F_o{}^2/\sigma^2(F^2)$), and an extinction correction of the form $F_{corr} = F_o(1 + sI_o)$. No reflections were rejected from the refinements. Final R values varied from 0.024 to 0.032. Values of the standard deviation of an observation of unit weight are listed in Table I as S. The final atom parameters listed in these tables were used with the variance–covariance matrices to calculate the interatomic distances and bond angles and their ESDs listed in Table II. Distances and angles for $(Ti_{0.9}V_{0.1})_2O_3$ were calculated from the cell parameters of this work and the atom parameters of Ref. (*25*). Structure factor amplitudes are reported in Table III.

Results

All of the Ti_2O_3–V_2O_3 alloys studied were found to be isomorphous with α-Al_2O_3. The structures consist of an approximate hexagonally closest packed array of oxide ions with metal ions occupying two-thirds of the octahedral interstices (Fig. 1). A given metal ion, $M(1)$, has four near-metal neigh-

TABLE II

INTERATOMIC DISTANCES (Å) AND BOND ANGLES (DEGREES) FOR $(Ti_{1-x}V_x)_2O_3$ WITH STANDARD DEVIATIONS IN PARENTHESES

	$x=0^a$	0.005	0.01	0.02	0.04	0.07	0.10	0.30	0.50	0.70	0.90	1.00[b]
						Distances						
M(1)–M(2)	2.578(2)	2.585(1)	2.595(1)	2.606(1)	2.627(1)	2.652(1)	2.659(1)	2.698(1)	2.708(1)	2.710(1)	2.713(1)	2.697(1)
M(1)–M(3)	2.994(1)	2.993(1)	2.990(1)	2.986(1)	2.978(1)	2.970(1)	2.967(1)	2.942(1)	2.921(1)	2.910(1)	2.901(1)	2.880(1)
M(1)–O(1)	2.066(1)	2.067(1)	2.069(2)	2.069(1)	2.070(1)	2.074(1)	2.072(1)	2.071(1)	2.066(1)	2.064(1)	2.059(1)	2.051(1)
M(1)–O(5)	2.027(1)	2.025(1)	2.023(1)	2.022(1)	2.017(1)	2.012(1)	2.012(1)	1.999(1)	1.988(1)	1.981(1)	1.977(1)	1.968(1)
O(1)–O(2)	2.796(1)	2.792(1)	2.792(3)	2.784(3)	2.772(2)	2.761(3)	2.752(1)	2.722(3)	2.703(3)	2.696(3)	2.683(2)	2.676(3)
O(1)–O(4)	2.791(1)	2.794(3)	2.794(3)	2.796(1)	2.799(1)	2.806(1)	2.806(1)	2.814(1)	2.813(1)	2.811(1)	2.807(1)	2.804(1)
O(1)–O(5)	2.880(1)	2.881(1)	2.884(1)	2.887(1)	2.890(1)	2.898(1)	2.900(4)	2.907(1)	2.904(1)	2.900(1)	2.989(1)	2.889(1)
O(4)–O(5)	3.073(2)	3.071(2)	3.068(2)	3.065(2)	3.057(1)	3.048(2)	3.047(1)	3.021(2)	2.998(2)	2.984(2)	2.977(2)	2.952(1)
						Angles						
O(1)–M(1)–O(2)	85.20(7)	85.05(5)	84.84(5)	84.57(5)	84.05(4)	83.48(5)	83.24(4)	82.16(5)	81.72(5)	81.55(5)	81.32(6)	81.45(7)
O(1)–M(1)–O(4)	85.96(2)	86.02(2)	86.13(2)	86.24(1)	86.44(1)	86.74(1)	86.80(5)	87.45(2)	87.84(2)	88.02(2)	88.10(2)	88.46(2)
O(1)–M(1)–O(5)	89.42(5)	89.50(4)	89.59(3)	89.76(4)	90.01(3)	90.32(4)	90.47(5)	91.14(4)	91.49(5)	91.60(4)	91.75(4)	91.90(5)
O(1)–M(1)–O(6)	170.01(8)	169.90(6)	169.78(7)	169.61(6)	169.26(5)	168.95(6)	168.78(10)	168.30(5)	168.20(4)	168.24(6)	168.10(7)	168.62(8)
O(4)–M(1)–O(5)	98.69(3)	98.61(3)	98.59(3)	98.56(2)	98.57(2)	98.48(3)	98.48(5)	98.16(2)	97.87(2)	97.74(2)	97.71(3)	97.17(3)
M(1)–O(1)–M(2)	77.18(9)	77.40(7)	77.67(7)	78.05(6)	78.75(6)	79.52(7)	79.84(1)	81.29(6)	81.88(7)	82.10(6)	82.41(7)	82.23(9)
M(1)–O(2)–M(3)	94.04(2)	93.98(2)	93.87(2)	93.76(1)	93.56(1)	93.26(2)	93.20(4)	92.55(2)	92.16(3)	91.98(2)	91.89(2)	91.54(3)
M(2)–O(2)–M(3)	132.33(5)	132.35(4)	132.37(4)	132.44(3)	132.52(3)	132.61(4)	132.69(8)	132.92(3)	133.04(4)	133.06(4)	133.14(4)	133.21(5)

[a] Ref. (*23*).
[b] Ref. (*26*).

TABLE III

VALUES OF 10 F_{obs} AND 10 F_{calc}.

			.5% V		1% V		2% V		4% V		7% V		30% V		50% V		70% V		90% V	
H	K	L	FOBS	FCALC	FOBS	FCALC	FOBS	FCALC	FOBS	FCALC	FOBS	FCALC	FOBS	FCALC	FOBS	FCALC	FOBS	FCALC	FOBS	FCALC
0	0	6	650	701	670	703	659	705	643	695	643	692	664	702	673	710	707	742	699	760
0	0	12	1077	1060	1120	1065	1090	1074	1062	1049	1076	1046	1072	1043	1055	1024	1097	1067	1078	1063
0	0	18	74	67	96	77	83	92	121	129	171	164	244	230	244	236	225	239	235	244
0	1	2	799	804	789	799	796	812	813	816	801	805	805	815	796	816	855	852	858	864
0	1	8	146	135	158	151	173	164	200	196	238	229	300	289	300	293	311	300	320	310
0	1	14	427	439	462	471	479	473	497	494	531	536	612	602	592	603	604	614	612	626
0	1	20	561	578	612	626	619	614	611	602	647	650	705	715	687	698	685	699	700	709
0	2	4	1137	1139	1127	1143	1155	1178	1196	1203	1202	1213	1227	1253	1220	1243	1347	1334	1346	1344
0	2	10	986	965	1007	981	997	997	1002	1000	1035	1018	1077	1055	1071	1043	1105	1095	1114	1103
0	2	16	838	824	873	856	842	847	825	823	846	842	878	863	849	852	852	863	854	868
0	3	6	650	653	652	656	664	658	653	650	647	641	639	639	648	645	657	652	658	663
0	3	12	807	807	906	879	861	873	863	845	846	830	804	808	809	801	812	808	806	803
0	3	18	54	44	49	53	61	67	110	99	121	130	176	188	179	192	182	193	186	196
0	4	2	548	553	552	554	563	559	559	553	533	543	534	534	531	536	531	531	533	535
0	4	8	165	168	178	179	190	190	207	209	232	229	267	266	269	268	267	265	268	272
0	4	14	294	290	305	319	311	310	330	333	352	360	387	397	386	408	400	401	397	409
0	5	4	734	731	735	744	762	753	771	755	745	747	761	746	753	766	771	758	764	762
0	5	10	653	660	662	678	670	680	671	671	672	669	673	673	679	676	671	667	672	675
0	6	6	460	491	490	499	490	497	479	488	465	468	462	452	456	469	452	444	456	453
1	0	4	1095	1141	1091	1144	1129	1180	1149	1204	1172	1219	1250	1268	1221	1260	1332	1371	1356	1385
1	0	10	1127	1115	1161	1131	1162	1157	1173	1171	1211	1195	1307	1247	1274	1230	1316	1317	1348	1327
1	0	16	815	800	849	830	834	821	809	794	819	814	863	838	825	821	831	835	840	840
1	1	0	1114	1200	1122	1196	1167	1234	1216	1254	1155	1256	1244	1291	1199	1284	1341	1396	1348	1414
1	1	3	772	737	768	737	790	747	776	748	795	748	778	747	769	740	802	757	797	753
1	1	6	1442	1415	1427	1413	1473	1462	1487	1477	1505	1478	1534	1505	1507	1477	1644	1618	1636	1620
1	1	9	443	452	461	455	463	456	453	451	455	454	469	456	457	456	460	457	459	455
1	1	12	496	496	509	501	486	486	450	451	434	436	407	407	401	401	401	397	402	398
1	1	15	261	274	275	278	270	275	262	267	264	271	276	275	269	275	262	271	260	268
1	1	18	334	339	345	337	313	314	268	264	238	237	185	183	179	176	181	165	166	156
1	2	2	535	530	533	528	531	528	523	519	513	508	497	497	503	502	496	505	502	506
1	2	5	119	117	124	116	124	119	126	118	125	119	128	126	129	122	125	118	128	120
1	2	8	53	44	60	57	68	66	89	91	118	116	158	157	168	164	176	168	174	173
1	2	11	69	73	71	72	71	75	72	72	76	73	79	79	77	75	75	72	74	73
1	2	14	422	434	452	463	462	466	476	483	511	518	565	574	561	576	576	578	585	589
1	2	17	46	50	50	49	46	50	52	46	47	47	52	53	51	49	52	47	55	47
1	3	1	81	79	83	80	81	81	82	79	81	79	84	80	92	84	80	79	80	78
1	3	4	757	751	754	758	778	769	791	775	778	774	780	783	800	788	801	804	804	811
1	3	7	70	67	71	69	72	68	68	69	71	69	71	70	67	76	74	71	65	71
1	3	10	913	902	934	922	951	933	945	935	956	943	973	964	977	965	992	988	997	995
1	3	13	51	50	55	54	58	52	53	53	60	54	57	54	65	60	61	57	71	57
1	3	16	672	677	697	707	681	694	677	663	668	672	658	679	658	671	655	662	660	666
1	4	3	277	280	281	285	286	284	276	277	271	274	261	263	262	266	256	261	261	257
1	4	6	947	925	951	933	970	946	958	935	938	920	925	904	922	911	936	920	919	921
1	4	9	227	236	235	241	236	239	227	231	225	230	230	223	226	226	223	220	219	216
1	4	12	388	398	395	406	385	392	363	363	340	345	311	316	308	316	306	301	300	303
1	5	2	262	267	268	270	262	266	252	256	244	243	232	227	232	237	227	226	226	226
1	5	5	109	115	112	116	112	119	109	117	115	117	120	119	116	120	111	113	109	114
1	5	8	34	7	28	3	23	7	40	23	52	36	65	58	67	65	78	64	73	67
1	5	11	91	99	96	100	92	102	94	98	96	98	--	--	--	--	--	--	--	--
1	6	1	62	64	61	66	67	67	57	62	56	60	--	--	--	--	--	--	--	--
2	0	2	532	530	530	528	528	526	511	519	491	509	443	496	497	500	491	511	505	514
2	0	8	17	9	42	17	32	26	61	57	83	86	129	127	144	137	142	144	152	152
2	0	14	476	486	501	507	519	513	524	528	561	566	630	631	630	628	637	635	652	645
2	1	1	149	140	153	141	153	144	152	146	154	146	155	151	155	150	147	146	150	149
2	1	4	1004	989	1002	994	1023	1020	1047	1036	1043	1043	1074	1069	1072	1063	1112	1119	1132	1128
2	1	7	99	105	100	108	101	106	103	111	107	113	113	116	116	118	113	114	114	117
2	1	10	953	934	967	952	983	965	965	967	988	981	1034	1012	1027	1006	1043	1045	1062	1053
2	1	13	67	69	70	72	70	71	67	73	70	75	71	77	95	80	66	77	69	79
2	1	16	779	774	811	806	801	796	771	769	786	784	794	801	781	789	785	792	795	797
2	2	0	960	963	970	964	992	984	1010	991	993	982	975	987	1005	991	1029	1027	1043	1036
2	2	3	400	404	406	407	406	408	401	401	394	398	385	388	391	390	384	386	377	381
2	2	6	1140	1102	1136	1106	1166	1130	1157	1128	1155	1119	1126	1117	1139	1109	1179	1158	1177	1159
2	2	9	302	305	307	309	305	307	302	300	292	300	289	295	297	298	281	293	278	289
2	2	12	426	436	439	442	421	427	392	395	377	378	340	349	341	348	333	336	336	337
2	2	15	210	223	224	228	217	224	211	215	209	217	211	216	211	218	209	212	206	209
2	3	2	309	308	306	310	305	05	301	298	281	287	276	271	280	276	267	272	268	274
2	3	5	85	83	83	84	90	86	86	86	86	87	89	89	89	87	88	85	89	87
2	3	8	51	23	20	12	30	8	44	17	39	35	62	61	76	68	79	71	88	77
2	3	11	63	66	64	66	62	68	65	67	65	68	70	71	70	69	71	67	71	68
2	3	14	400	415	422	441	429	445	447	451	472	476	496	520	516	524	518	513	520	520
2	4	1	105	107	108	109	109	110	107	108	106	107	105	108	109	113	104	105	103	105
2	4	4	614	620	618	631	634	637	639	639	627	631	620	627	639	639	618	629	624	636
2	4	7	97	100	101	104	102	103	102	103	101	103	101	103	112	111	109	103	104	103
2	4	10	707	712	722	735	730	736	740	728	719	725	719	725	732	742	719	728	720	733
2	5	3	176	178	180	184	175	182	175	173	162	168	156	158	162	165	155	158	156	153
2	5	6	740	744	756	758	768	762	745	746	720	723	--	--	--	--	--	--	--	--
3	0	0	1551	1548	1588	1544	1650	1608	1679	1635	1652	1630	1642	1652	1640	1620	1814	1787	1792	1786
3	0	6	654	653	654	656	653	657	641	650	629	641	633	639	649	644	648	652	656	662
3	0	12	885	867	898	876	896	874	831	841	837	831	811	809	804	802	816	808	810	804
3	0	18	38	44	54	54	60	68	85	100	126	131	180	185	182	193	187	194	194	197
3	1	2	540	540	548	540	549	543	546	535	524	525	518	516	524	519	508	515	516	518
3	1	5	68	69	68	68	69	70	69	65	66	65	72	68	69	69	66	64	68	63
3	1	8	130	126	145	137	149	147	170	167	186	188	224	226	235	230	231	228	242	234
3	1	11	45	49	41	47	52	49	42	44	43	43	47	49	51	46	48	42	51	41
3	1	14	336	340	368	369	365	369	375	386	406	415	452	458	454	466	454	462	465	471
3	1	17	33	35	41	33	28	35	33	29	33	29	32	33	38	30	39	28	41	26
3	2	1	89	90	89	91	92	93	91	95	92	95	94	97	94	96	90	93	90	95
3	2	4	807	792	810	803	829	816	833	822	823	818	819	823	838	834	833	841	841	847
3	2	7	77	79	79	81	79	82	78	83	80	84	80	85	75	85	72	83	76	84
3	2	10	723	723	734	741	741	745	730	738	729	740	745	749	743	752	748	752	752	758
3	2	13	59	63	66	65	58	65	68	66	64	67	74	69	72	69	69	67	67	68
3	3	0	1090	1056	1099	1084	1118	1089	1132	1088	1091	1068	1063	1051	1091	1062	1091	1083	1086	1082
3	3	3	15	4	17	4	18	4	23	6	14	6	42	6	18	3	33	5	25	7
3	3	6	528	527	532	534	528	532	518	524	505	506	493	494	500	506	497	488	500	497
3	3	9	21	3	21	3	31	4	27	5	31	7	25	5	27	3	29	4	28	6
3	3	12	667	671	675	685	671	675	741	638	615	619	571	584	579	592	567	573	562	567
3	4	2	398	408	400	414	401	416	393	406	380	392	371	378	379	390	360	370	363	372
3	4	5	28	28	24	27	24	28	23	24	24	23	26	24	30	26	27	22	30	31
3	4	8	147	146	149	156	162	165	167	176	--	--	--	--	--	--	--	--	--	--
4	0	4	652	652	663	660	676	665	664	667	653	664	648	666	688	677	678	682	688	686
4	0	10	912	897	934	918	941	930	944	931	930	938	959	956	977	958	972	975	984	983
4	0	16	617	627	640	657	644	642	589	609	608	616	607	618	592	614	594	600	599	603
4	1	0	831	815	837	820	846	832	848	834	824	819	828	813	845	823	833	828	842	837
4	1	3	284	281	286	285	283	284	280	278	275	274	257	263	262	267	250	261	250	257
4	1	6	949	925	966	934	973	946	948	936	933	920	907	904	933	912	919	921	928	921
4	1	9	233	236	235	241	237	239	227	232	230	231	222	224	228	227	221	222	218	218
4	1	12	390	398	397	405	382	392	358	362	333	344	304	315	312	315	301	300	311	302
4	2	2	333	339	338	341	342	339	325	328	310	315	295	300	307	311	293	297	296	297
4	2	5	94	99	96	99	97	102	96	97	96	95	98	99	98	101	91	94	96	92
4	2	8	49	47	56	55	73	62	87	75	91	89	115	115	130	121	124	117	132	120
4	2	11	77	83	82	82	82	85	77	77	77	76	75	81	82	80	78	74	70	73
4	3	1	31	31	33	32	26	32	37	29	34	28	26	28	39	32	22	29	29	27
4	3	4	444	457	462	468	459	468	452	465	442	453	440	442	450	461	433	442	441	447
4	3	7	27	30	35	33	34	32	34	31	31	30	37	29	23	35	27	31	--	--
5	0	2	261	260	260	262	260	257	247	254	240	243	223	226	227	229	217	225	221	229
5	0	8	45	35	27	23	52	20	52	8	61	24	50	45	54	51	98	55	111	62
5	1	1	117	121	124	124	123	126	121	126	122	126	123	126	125	129	119	122	114	123
5	1	4	648	647	658	660	666	667	663	668	651	659	652	654	664	670	641	656	663	663
5	1	7	111	113	113	117	115	118	116	119	119	119	117	119	119	123	116	117	116	118
5	1	10	641	647	656	669	660	668	650	658	640	652	644	649	659	666	636	647	651	653
5	2	0	656	655	663	665	662	670	664	665	634	641	626	623	643	649	623	623	641	629
5	2	3	173	179	176	184	177	183	170	174	165	170	159	159	161	166	154	159	154	154
5	2	6	753	744	761	759	760	762	745	747	721	724	718	694	--	--	--	--	--	--
6	0	0	954	940	981	953	978	970	980	962	949	938	941	912	938	934	938	930	947	929
6	0	6	479	490	487	498	491	496	486	486	463	466	463	450	460	466	447	441	444	450
6	1	2	329	338	339	344	328	343	323	331	310	316	--	--	--	--	--	--	--	--

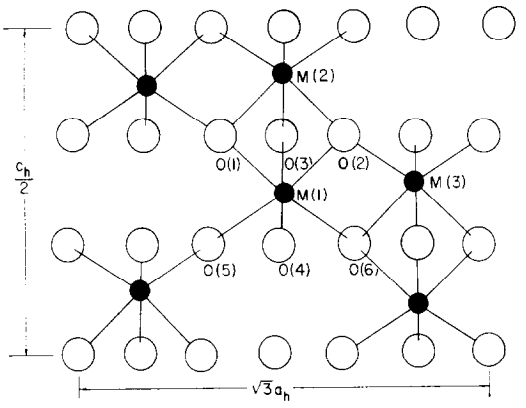

FIG. 1. A projection of the corundum structure on a plane perpendicular to the [110] axis.

bors; one sharing a triangular face of the coordination octahedron [$M(2)$ in Fig. 1] and three sharing edges of the octahedron [$M(3)$ in Fig. 1].

The values of the unit cell parameters in the Ti_2O_3–V_2O_3 system at various compositions are shown in Table I and in Fig. 2. The

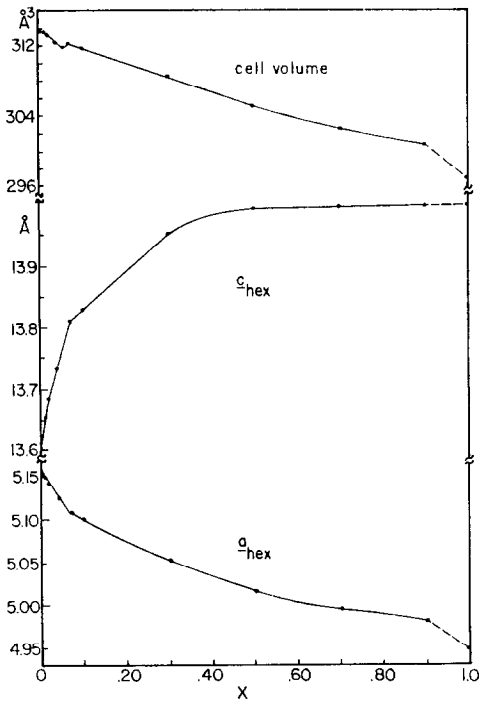

FIG. 2. Variation of unit cell parameters and cell volume in $(Ti_{1-x}V_x)_2O_3$.

data shown for Ti_2O_3 and V_2O_3 have been taken from Refs. (*23*, *26*), respectively. Many unit cell determinations (*33*) and several refined crystal structures of Ti_2O_3 and V_2O_3 from single crystal data (*22–27*) are available. With the exception of the V_2O_3 parameters, all parameters reported were determined on the same instrument under the same conditions and thus comparisons of small changes should not be affected by possible systematic errors between equipment or by differences in conditions. The V_2O_3 distances and angles of Refs. (*26*, *27*) are identical within 2 ESDs.

Adding V_2O_3 to Ti_2O_3 causes rapid changes in both axes in the low-vanadium region, with less pronounced changes at higher concentrations. Over half of the change in the c axis occurs between 0 and 7 at. % of V. Additionally, a plot of c axis length vs vanadium concentration is approximately linear from 0–2 and from 2–7% V, with a slight change in slope between these regions. There is a quite noticeable break in slope in the vicinity of 7% V. The c axis then increases more slowly, finally leveling off in the 50–100% V region. The a axis decreases abruptly between 0 and 7% V. Like the c axis, a varies linearly with composition from 0–2 and 2–7% V. A similar break in the slope of the a vs % V plot is seen around 7% V. Unlike c, the a axis does not level off but rather decreases throughout the entire composition range. A positive deviation from Vegard's law is observed for the a axis in the vicinity of 90% V. The behavior for $x = 0.9$ is consistent with that observed for $0.92 \leqslant x \leqslant 1.0$ (*34*).

As well as can be seen (only figures are presented), our cell constant data agree with the results of Kawabuko, Yanagi, and Nomura (*21*) and Loehman, Rao, and Honig (*5*). However, these earlier studies were carried out with rather limited data sets and so are not as precise and do not show as much detail as the present work. For example, our plot of cell volume vs concentration (Fig. 2) shows an unusual S-shaped wiggle between 0 and 10 at. % of V, a feature which had not been noticed before.

The c/a ratios of both Ti_2O_3 and V_2O_3 are unusual when compared to those of most corundum-like oxides (*35*). While α-Al_2O_3,

α-Fe_2O_3, α-Cr_2O_3, Rh_2O_3, and Ga_2O_3 all have c/a ratios falling in the range 2.70–2.74, the Ti_2O_3 c/a ratio is abnormally small at 2.64; V_2O_3 shows the anomalously large value of 2.83. Rapid approaches toward more "normal" values of the c/a ratio are seen at both extreme ends of the composition scale (Table I).

The major change in the atomic coordinates of the $(Ti_{1-x}V_x)_2O_3$ system occurs in the metal z parameter. The z parameter for the metal atom at $(0,0,z)$ increases by some 57 ESDs (Table I). As with the c axis, over half of this change occurs in the 0–7 at. % of V region. z also shows linear increases from 0–2 and 2–7% V, followed by less rapid changes at higher vanadium concentrations. Unlike the c axis, which remains constant from 50 to 100% V, z decreases from $(Ti_{0.1}V_{0.9})_2O_3$ to pure V_2O_3.

The oxygen x parameter changes no more than 5 to 7 ESDs throughout the entire composition range. Having virtually the same value in Ti_2O_3 and V_2O_3 x drops slightly in the alloys.

The thermal parameters are well behaved and have reasonable values for systems of this sort; however, they do not vary with composition in any coherent way. It should be mentioned that these crystals exhibit rather strong extinction, which has substantial effects on the temperature factor refinement (*23*). Extinction effects depend to some degree on crystal size. Thus, the use of crystals of different sizes causes enough scatter in the β_{ij}'s to obscure evidence of any subtle trends.

The changes in metal–metal distances caused by the changes in cell parameters and fractional atomic coordinates are shown in Table II and Fig. 3. The distance between metal ions sharing an octahedral face of their coordination polyhedra, $M(1)$–$M(2)$, increases sharply from 2.578(1) Å in Ti_2O_3 to 2.652(1) Å in $(Ti_{0.93}V_{0.07})_2O_3$, then more slowly to a maximum of 2.713(1) Å in $(Ti_{0.1}V_{0.9})_2O_3$, a total increase of 5.4% (the c axis increases by 2.9% over the same concentration range). The $M(1)$–$M(2)$ distance then decreases to 2.697(1) Å in V_2O_3. The distance between edge-sharing metal neighbors, $M(1)$–$M(3)$, decreases continuously from 2.994(1) Å

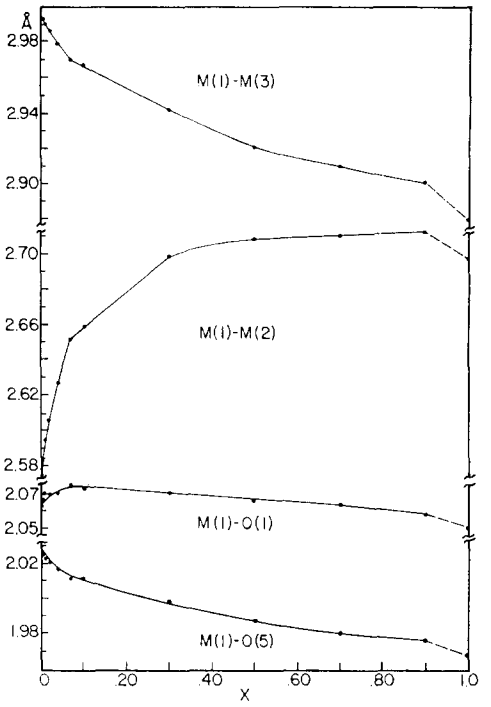

FIG. 3. Variation of metal–metal and metal–oxygen distances in $(Ti_{1-x}V_x)_2O_3$.

in Ti_2O_3 to 2.880(1) Å in V_2O_3, a 3.8% change, while a decreases by 4.0%. Both the $M(1)$–$M(2)$ and $M(1)$–$M(3)$ distances depend linearly on composition from 0–2 and 2–7% V; plots of both distances vs. % V show distinct breaks in slope in the vicinity of 7 at % V.

The effects of changing composition on the metal–oxygen and oxygen–oxygen distances are also shown in Table II and in Fig. 3. The 0–7% V concentration range will be discussed first. In these alloys, the distance from $M(1)$ to an oxygen in the shared octahedral face, $M(1)$–O(1), indreases from 2.062(1) Å in Ti_2O_3 to 2.074(1) Å in $(Ti_{0.93}V_{0.07})_2O_3$. At the same time, the distance between oxygens in this shared face, O(1)–O(2), decreases from 2.791(1) to 2.761(3) Å. Thus as $M(1)$ and $M(2)$ move apart, their shared oxygens move closer together. The distance from $M(1)$ to an oxygen in the opposite octahedral face, $M(1)$–O(5), decreases from 2.028(1) Å in Ti_2O_3 to 2.012(1) Å in $(Ti_{0.93}V_{0.07})_2O_3$ as

$M(1)$ approaches this face. The distance between oxygens in this unshared octahedral face, O(4)–O(5), also decreases with increasing vanadium content. Distances between oxygens in different closest packed layers, such as O(1)–O(4) and O(1)–O(5), show significant increases, as expected from the substantial increase in the c axis observed for this concentration range.

In the composition range from 7 to 90% vanadium, the $M(1)$–$M(3)$ distance continues to decrease and $M(1)$–$M(2)$ to increase, although in a more gradual manner than at lower vanadium concentrations. The metal–oxygen bonded distances decrease, reflecting the diminishing average size of the metal ion (*36*). Distances between oxygens in the same closest-packed layer, O(1)–O(2) and O(4)–O(5), continue to decrease, paralleling the a axis behavior. The interlayer oxygen–oxygen distances change little in this range.

Although no data other than cell dimensions (*34*) is yet available for samples in the concentration range 90–100% V_2O_3, plainly there are structural changes here which are not continuations of the middle concentration range behavior. After essentially leveling off in the 50–90% V range, both $M(1)$–$M(2)$ and $M(1)$–$M(3)$ drop significantly from 90–100% V. The metal–oxygen distances decrease more steeply in this range than at lower vanadium concentrations. Among the oxygen–oxygen distances, O(1)–O(5) and O(4)–O(5) decrease rapidly between 90 and 100% V, but no unusual changes are seen in O(1)–O(4) or O(1)–O(2).

Discussion

The structural behavior observed in the Ti_2O_3–V_2O_3 system as the composition changes cannot be explained by Vegard's law. The deviations from this law are especially striking in the low-vanadium alloys. In this composition range the interatomic distance changes are too great to be due to changes in ionic size; in fact, many of these distances change in the opposite direction to that expected from size considerations. Thus the structural changes caused by adding small amounts of V_2O_3 to Ti_2O_3 must be due in large part to electronic effects related to the semiconductor–metal transition which occurs in lightly vanadium-doped Ti_2O_3 with increasing dopant concentration.

Ti_2O_3 is a semiconductor at room temperature, although a transition to metallic behavior occurs in the 150–350°C temperature range (*2*, *3*). Adding increasing amounts of V_2O_3 to Ti_2O_3 successively lowers the room temperature resistivity of the alloy and decreases the magnitude of the resistivity drop across the semiconductor–metal transition without changing the transition temperature range (*1*). With the vanadium content somewhat greater than 2 at%, the alloy becomes metallic at all temperatures, though a small resistivity drop is still seen in the 150–350°C range. At about 7% V, this high-temperature transition disappears, and the room temperature resistivity becomes insensitive to vanadium content.

The greatest changes in all structural parameters in $(Ti_{1-x}V_x)_2O_3$ occur as x varies from 0 to 0.07. This is the composition range where electrical measurements show a decrease in resistivity and disappearance of the high-temperature resistivity anomaly. Several interatomic distances in these low-vanadium alloys change significantly with doping. However, as with the structural changes observed in Ti_2O_3 upon heating (*22*, *23*), these structural changes can be described satisfactorily as the result of an increase in the $M(1)$–$M(2)$ distance coupled with reorganization of the structure in order to minimize changes in metal–oxygen distances. As $M(1)$ and $M(2)$ move apart, their shared oxygens move together to counteract the lengthening of the $M(1)$–O(1) distance, and the oxide layers move apart so that $M(1)$–O(5) remains reasonably constant. Thus the lengthening of the c axis with increasing vanadium content is caused by the increase in the $M(1)$–$M(2)$ distance, while the contraction of the a axis reflects the inward motion of O(1), O(2), and O(3) as they follow the metal motion. The decrease in the $M(1)$–$M(3)$ distance is small, and can be ascribed to the movement of the shared oxygen toward $M(1)$, pulling $M(3)$ along with it. Thus we

see that large changes in the $M(1)$–$M(2)$ distance at room temperature accompany the diminution and disappearance of the resistivity drop which occurs between 150 and 350°C in lightly vanadium-doped Ti_2O_3. Interestingly, the plots of many structural parameters vs % V also show a slight change in slope around 2 at% V, the composition corresponding to the onset of metallic behavior in the alloys.

The temperature-induced semiconductor–metal transition in pure Ti_2O_3 has been explained (*13*, *14*, *37*) in terms of a band-crossing model. In the proposed Ti_2O_3 band structure the valence band, a band of a_1 symmetry, is formed by the bonding interaction between d_{z^2} orbitals of c axis neighbor metal ions, $M(1)$ and $M(2)$. This band is completely filled at 0°K. At low temperatures, the valence band is separated by a small gap from the conduction band, of e symmetry, which is formed by overlapping d orbitals of edge-sharing metal neighbors in the basal plane, $M(1)$ and $M(3)$. As Ti_2O_3 is heated, electrons are thermally promoted across the gap from the a_1 to the e band. The resulting loss of electron density from the a_1 band causes a weakening and lengthening of the $M(1)$ $M(2)$ bond. As this distance increases, the a_1 band is destabilized and so rises in energy until it crosses the e band, at which point Ti_2O_3 becomes metallic.

In vanadium-doped Ti_2O_3, vanadium is known to act as an acceptor or p-type dopant (*7*). This behavior would also remove electrons from the valence band. Thus the same band shifts and atomic movements expected for pure Ti_2O_3 when it is heated should also occur with vanadium doping.

The increase observed in the $M(1)$–$M(2)$ distance in $(Ti_{1-x}V_x)_2O_3$ as x increases from 0 to 0.07 is in agreement with structural predictions based on the band-crossing model. The changes in structural behavior which occur for $0 \leqslant x \leqslant 0.02$ can be understood if it is assumed that acceptor impurity levels introduced by V_2O_3 lie in the a_1–e band gap of Ti_2O_3. Thus as increasing vanadium content weakens the $M(1)$–$M(2)$ bond and causes the a_1 band to rise in energy, the a_1 band crosses these impurity levels, resulting in metallic behavior for $(Ti_{0.98}V_{0.02})_2O_3$. The existence of a narrow level within the a_1 band has been postulated by Van Zandt (*20*) to account for the anomalous low-temperature specific heat observed for vanadium concentrations of 2 at% V and greater. As the vanadium concentration increases to about 7%, the a_1 and e bands cross, and the high-temperature resistivity drop disappears. Thus the electrical transition observed at about 7% vanadium is analogous to the temperature-induced semiconductor-metal transition in pure Ti_2O_3. Accordingly, the interatomic distances in $(Ti_{0.93}V_{0.07})_2O_3$ are almost identical to those in Ti_2O_3 at 350°C (*22*, *23*), when allowance is made for the effects of ionic size and thermal expansion.

As the vanadium content in Ti_2O_3–V_2O_3 alloys increases from 7 at% V, the $M(1)$–$M(2)$ distance and the c axis increase more gradually than at lower concentrations, then level off at approximately 50% V. This behavior is consistent with a band model for V_2O_3 in which the e band is proposed to lie below the a_1 band in energy (*38*); this order is the reverse of that in Ti_2O_3. Thus the a_1 band in Ti_2O_3 alloys is gradually destabilized with respect to the e band as the vanadium content increases, resulting in the observed increase in the $M(1)$–$M(2)$ distance. The leveling off of $M(1)$–$M(2)$ at 50% V could result if the a_1 band in this alloy has risen in energy enough to be essentially unpopulated, so that further energy shifts cause negligible changes in bond order.

Apart from the c axis and $M(1)$–$M(2)$ distance behavior, the structural changes in $(Ti_{1-x}V_x)_2O_3$, $0.07 \leqslant x \leqslant 0.90$, can be explained rather well by the effects of changing effective ionic size. However, our limited data suggest that sime unusual structural behavior occurs in the 90–100% V range. It has been observed that adding small amounts of Ti_2O_3 to V_2O_3 has drastic effects on the insulator–metal transition which occurs in pure V_2O_3 at 150°K (*39*). Though the effect of Ti doping on the room temperature resistivity of these alloys is rather minor, evidently some structural changes do result. Interpretation of these changes awaits more detailed structural study of this composition region (*40*).

Acknowledgments

We would like to thank Professor J. M. Honig for providing samples and for enlightening discussions, George Yuochonas for the growth of crystals used in this work, and the Stauffer Chemical Company for award of a fellowship to C.E.R. This work was supported by the National Science Foundation NSF-MRL Program DMR-7203018-A04.

References

1. G. V. Chandrashekhar, Q. Won Choi, J. Moyo, and J. M. Honig, *Mater. Res. Bull.* **5**, 999 (1970).
2. F. J. Morin, *Phys. Rev. Lett.* **3**, 34 (1959).
3. J. Yahia and H. P. R. Frederikse, *Phys. Rev.* **123**, 1257 (1961).
4. L. J. Eckert and R. C. Bradt, *J. Appl. Phys.* **44**, 3470 (1973).
5. R. E. Loehman, C. N. R. Rao, and J. M. Honig, *J. Phys. Chem.* **73**, 1781 (1969).
6. J. M. Honig and T. B. Reed, *Phys. Rev.* **174**, 1020 (1968).
7. S. H. Shin, G. V. Chandrashekhar, R. E. Loehman, and J. M. Honig, *Phys. Rev. B* **8**, 1364 (1973).
8. H. L. Barros, G. V. Chandrashekhar, T. C. Chi, J. M. Honig, and R. J. Sladek, *Phys. Rev. B* **7**, 5147 (1973).
9. A. Mooradian and P. M. Raccah, *Phys. Rev. B* **3**, 4253 (1971).
10. S. H. Shin, R. L. Aggarwal, B. Lax, and J. M. Honig, *Phys. Rev. B* **9**, 583 (1974).
11. T. C. Chi and R. J. Sladek, *Phys. Rev. B* **7**, 5080 (1973).
12. J. G. Bennett and R. J. Sladek, *Solid State Commun.* **18**, 1055 (1976).
13. J. B. Goodenough, *Phys. Rev.* **117**, 1442 (1960).
14. J. B. Goodenough, "Magnetism and the Chemical Bond," Interscience, New York, (1963).
15. M. E. Sjöstrand and P. H. Keesom, *Phys. Rev. B* **7**, 3558 (1973).
16. J. Dumas, C. Schlenker, and R. C. Natoli, *Solid State Commun.* **16**, 493 (1975).
17. J. Dumas, C. Schlenker, J. L. Tolence, and R. Tournier, *Solid State Commun.* **17**, 1215 (1975).
18. L. L. Van Zandt, J. M. Honig, R. E. Loehman, O. P. Katyal, D. A. Lilly, L. W. Lonney, and P. H. Keesom, *Phys. Rev. Lett.* **22**, 946 (1969).
19. N. F. Mott and L. Friedman, *Philos. Mag.* **30**, 389 (1974).
20. L. L. Van Zandt, *Phys. Rev. Lett* **31**, 598 (1973).
21. T. Kawakubo, T. Yanagi, and S. Nomura, *J. Phys. Soc. Japan* **15**, 2102 (1960).
22. C. E. Rice and W. R. Robinson, *Mater. Res. Bull.* **11**, 1355 (1976).
23. C. E. Rice and W. R. Robinson, *Acta Crystallogr.* in press.
24. R. E. Newnham and Y. M. de Haan, *Z. Krist.* **117**, 235 (1962).
25. W. R. Robinson, *J. Solid State Chem.* **9**, 255 (1974).
26. W. R. Robinson, *Acta Crystallogr. B* **31**, 1153 (1975).
27. P. D. Dernier, *J. Phys. Chem. Solids* **31**, 2569 (1970).
28. W. H. Zachariasen, *Acta Crystallogr.* **18**, 705 (1965).
29. D. E. Williams, "LCR-2, a Fortran IV Lattice Constant Refinement Program," IS-1052, Iowa State University, Ames, Iowa, 1964.
30. L. W. Finger, "RFINE-2, a Fortran IV Program for Structure Factor Calculation and Least-Squares Refinement of Crystal Structures," Geophysical Laboratory, Washington, D.C., 1972.
31. D. T. Cromer and J. T. Waber, *Acta Crystallogr.* **18**, 104 (1965).
32. D. T. Cromer, *Acta Crystallogr.* **18**, 17 (1965).
33. "Landolt-Börnstein, New Series, Group III," (K. H. Hellwege and A. M. Hellwege, Eds.), Vol. 7b, pp. 299 and 417. Springer-Verlag, Berlin, 1975.
34. D. B. McWhan, A. Menth, J. P. Remeika, W. F. Brinkman, and T. M. Rice, *Phys. Rev. B* **7**, 1920 (1973).
35. C. T. Prewitt, R. D. Shannon, D. B. Rogers, and A. W. Sleight, *Inorg. Chem.* **8**, 1985 (1969).
36. R. D. Shannon and C. T. Prewitt, *Acta Crystallogr. B* **25**, 925 (1969).
37. L. L. Van Zandt, J. M. Honig, and J. B. Goodenough, *J. Appl. Phys.* **39**, 594 (1968).
38. J. B. Goodenough, *Prog. Solid State Chem.* **5**, 145 (1971).
39. D. B. McWhan, J. P. Remeika, T. M. Rice, W. F. Brinkman, J. P. Maita, and A. Menth, *Phys. Rev. Lett* **27**, 941 (1971).
40. C. E. Rice and W. R. Robinson, to appear.